C. R. Physique 3 (2002) 273–288

Solides, fluides : structure/*Solids, fluids: structure*
(Atomes, molécules/*Atoms, molecules*)

DOSSIER

AGRÉGATS COMME PRÉCURSEURS DES NANO-OBJETS
CLUSTERS AS PRECURSORS OF NANO-OBJECTS

Covalent clusters-based materials

Patrice Mélinon [a], Bruno Masenelli [a], Alain Perez [a], Michel Pellarin [b], Michel Broyer [b]

[a] **Département de physique des matériaux, Université Claude Bernard-Lyon 1, 69622 Villeurbanne, France**

[b] **Laboratoire de spectrométrie ionique et moléculaire, Université Claude Bernard-Lyon 1, 69622 Villeurbanne, France**

Received 15 October 2001; accepted 10 January 2002

Note presented by Guy Laval.

Abstract We review the properties of covalent clusters-based materials in relation to free cluster properties, namely carbon, silicon and mixed carbon clusters. These properties are understood in terms of quantum size especially the so called rehybridization effect. We show that low energy cluster beam deposition is a powerful technique to prepare unusual bonding. ***To cite this article: P. Mélinon et al., C. R. Physique 3 (2002) 273–288.*** © 2002 Académie des sciences/Éditions scientifiques et médicales Elsevier SAS

covalent cluster / quantum size

Matériaux covalents produits des d'agrégats

Résumé Des matériaux covalents sont produits à partir du dépôt d'agrégats de carbone, silicium voire d'agrégats mixtes silicium–carbone. Ces agrégats préformés en phase gazeuse sont issus d'une source à vaporisation laser. Les films sont produits par la technique LECBD (Low Energy Cluster Beam Deposition, dépôt à faible énergie). Suivant la nucléation dans la source, différents isomères sont obtenus, isomères ayant des propriétés électroniques différentes. La structure des films est sondée par différentes techniques : spectroscopies Auger et de photo émission X, Raman, absorption X près du seuil (XAS, EXAFS),... Dans le cas d'agrégats ayant la forme d'une « cage », la plupart des propriétés peuvent être discutées en termes de réhybridation. Les exemples discutés montrent que l'on peut obtenir des films dont les caractéristiques sont très différentes des phases massives correspondantes. Ces propriétés sont d'une part liées l'élaboration d'agrégats dans des conditions hors équilibre thermodynamique et d'autre part, aux effets quantiques de tailles. ***Pour citer cet article : P. Mélinon et al., C. R. Physique 3 (2002) 273–288.*** © 2002 Académie des sciences/Éditions scientifiques et médicales Elsevier SAS

agrégats covalents / effets quantiques de tailles

E-mail address: Patrice.Melinon@dpm.univ-lyon1.fr (P. Mélinon).

S1631-0705(02)01316-6/FLA

1. Introduction

There is currently an interest in producing new materials comprised of small covalent clusters. Starting from a piece of the bulk phase, the question addressed is: what happens when the size decreases continuously? New properties called 'size effects' appear. These size effects can be arbitrary classified following the size of the cluster. First of all, size resonance is expected when the particle diameter is of the same order of magnitude as the wavelength of an external excitation. Decreasing further, a confinement effect associated to the exciton localization appears. This is well known in CdS nanoparticles, nanoporous silicon or aromatic rings in carbon, and leads to interesting photophysics properties such as luminescence [1]. This is associated to a bandgap increase due to a level splitting. Finally, for the smallest sizes, the cluster inner structure changes totally. This is emphasized by the so called 'thermodynamic instability' of the silicon diamond below 2 nm range [2] (the silicon becomes 'amorphous-like') and the C_{60} fullerene [3] for carbon. This is the intermediate regime between the molecule and the solid. This quantum size effect, which will be the focus in this report, opens new fields in mechanical, electronic and optical devices. For example, fifty years ago, most people thought that in normal conditions carbon and silicon had an electronic structure well described in terms of sp^2 and sp^3 hybridization, respectively. Silicon crystallizes in diamond or hexagonal structures while carbon rather crystallizes in hexagonal planar lattice (graphite). Thirty years ago, Cros et al. [4] reported a new structure for silicon called 'clathrate' based on a particular distribution of silicon tetrahedra that results in face-sharing covalent cages (belonging to the fullerene family). These new crystalline forms present some interest owing to their structures. They have a large number of five fold rings and may be doped by intercalated atoms inside the cages. Likewise, twenty years ago, Smalley et al. [3] discovered a new kind of carbon called fullerene. These new forms derived from the graphite were characterized by a spheroidal structure with an empty core. All these news forms of carbon and silicon exhibit a striking similarity, a cage like structure. This cage-like form ensures a spherical shape that minimizes the number of atoms located at the surface. This is the driving force which explains these new forms.

This paper is divided in three parts. In the first, we report the case of carbon and the so called 'memory effect'. In the second part, we discuss the case of silicon clusters and the connection with the clathrate structure. Finally, we present some examples of new bonding through the association of carbon and silicon.

2. LECBD films

Nanostructured thin films can be prepared by deposition of free neutral clusters [5] (Low Energy Cluster Beam Deposition, LECBD). One has to consider several mechanisms occurring during growth. When free clusters collide with the substrate, they can fragment or re-evaporate upon impact. If their kinetic energy gained during the expansion is low enough (lower than the bond energy), no fragmentation occurs. This is the first assumption of the LECBD. Afterwards, deposited clusters move more or less on the substrate and collide among themselves. Assuming a low diffusion, the first monolayer is composed of a high density of randomly distributed isolated particles [6]. Conversely, for a large diffusion, the first monolayer will be composed of large ramified islands whose branches are made of the juxtaposition of individual particles resulting from the coalescence of several incident clusters [7]. However, even though the morphology depends on the nature of the substrate, the structure of a thin film formed by several cluster monolayers will be weakly influenced by diffusion. The reason is the following: far away from the percolation threshold (coverage rate $> 50\%$) most of the clusters touch each other, leading to an homogeneous network and we lack the initial morphology (ramified islands or isolated clusters). Secondly, once the first monolayer has filled, clusters are deposited onto the first cluster monolayer, minimizing the role of the substrate. Nevertheless, the most important parameter is the coalescence. If two (or more) abutting clusters do not merge, the quasi complex is not at the equilibrium state since its surface/volume ratio is prohibitive. Then, a complex diffusion mechanism leads to a new single particle after merging. This is of importance since this effect destroys the nanogranular structure. In other words, the films are always metastable. However,

the life time of the quasi complex is related to an activation energy. This energy is weak enough for metals but much higher for a covalent lattice owing to a strong cohesive bond energy.

3. Theoretical aspects

A comprehensive study of covalent cluster based materials is not so easy. The films present two disorder scales. First of all, deposited neutral clusters have a spread of size (and composition for mixed clusters). Secondly, the ballistic mode gives rise to a disordered system since the clusters are randomly distributed. It seems naturel to compare the LECBD films with usual amorphous covalent structures, namely a-C, a-Si and a-SiC compounds. However, the growth processes differ strongly. Neutral clusters are prepared in UHV without a reactive gas (H_2, N_2, ...). Moreover, the granular structure leads to a very low film density (half or less the density of standard amorphous compounds). The coordinance of the atoms will be strongly affected. The main difference is the growth process. Neutral clusters present their own electronic structure which differs from the bulk one. The description in terms of the hybridization ratio basically used in the physics of amorphous compounds does not hold for clusters.

3.1. Carbon

3.1.1. *Fullerenes*

Atomic carbon has six electrons: two core $1s$ and four valence electrons leading to the $s-p$ hybridization. Since the $2p$ orbital is as compact as the $2s$ orbital, carbon presents several sp mixing and consequently a wide variety of isomers. For the smallest sizes up to 10 atoms, the stable structure is linear. Increasing the size, there is a competition between linear, cycles and planar structures [8,9]. Above 20 atoms, carbon takes 2D or 3D shapes. The 3D shape corresponding to the fullerene structure becomes more stable above $N = 32$ atoms. Nevertheless, the stability of small fullerenes down to 20 atoms (a piece of the clathrate structure) is questionable. The electronic structure of fullerenes has been extensively discussed in the literature [10]. Our purpose is simply to discuss the basic tools for interpreting our results. The cluster shape depends on the competition between the strain energy cost and the energy gained if we remove surface atoms. Starting from the stable phase structure in normal conditions, namely a piece of graphite, the cohesive energy per atom will be drastically reduced by the under coordinated atoms located at the 'frontier' (i.e. the surface). Introducing pentagons leads to a convex curvature allowing the closing of the frontier by connecting the 'surface' atoms among themselves. All the atoms will be three-fold coordinated but the curvature introduces strain energy. This latter results from bond length and bond angle deviations from their ideal values. In addition, five fold rings introduce another effect related to the frustration. After reconstruction, these clusters named fullerenes have an empty core and a spheroidal shape. Pi Orbital Vector Axis analysis [11] (POAV) gives the mean hybridization $\bar{n}$ versus the cluster radius:

$$\bar{n} = 3\left(1 - \frac{12 \times \pi \times 20 \times 3^{3/2}}{1 - 12 \times \pi 3^{3/2}(20 + 2F_6)}\right) \tag{1}$$

where F_6 is the number of six-fold rings in the fullerene. We have to mention that the hybridization $\bar{n}$ reported here is not related to a tetrahedrally-bonded atom as defined in crystalline networks, but is related to the dihedral angle making the bond. This is of importance for the following discussion.

3.1.2. *V DOS in amorphous carbon*

The structure of the amorphous carbon is often deduced from the measurement of the hybridization. The structure depends on the method of preparation and the presence (or not) of some dopants (hydrogen, nitrogen, ...). The hybridization is well probed by Raman and x-ray photoemission (XPS) spectroscopies correlated together. The first gives the assignation of a band and the second the yield of each contribution (sp^2 and sp^3 hybridized atoms). Even though the Raman spectroscopy is not a safe way to get the true

hybridization, Raman spectra give qualitatively the nature of the bonding. If the short range order is comparable with the Raman coherence length, the selection rules are broken and the first Raman signal gives more or less the total vibrational density of states (V DOS). This leads to two Raman bands assigned to the graphite component G band located at 1560 cm^{-1}) and the so called disorder band labelled D located near 1350 cm^{-1}); see [12] and references therein. Formally, this holds essentially for glassy carbon [12]. The D band is related to the sixfold ring breathing mode of A_{1g} symmetry becoming active in small graphite clusters. In most amorphous carbon networks, these bands are more and less broadened, indicating a strong complexity of the carbon bonding inside the network. Strictly, one has to consider the collective features of both the sp^2 and the sp^3 atoms (and sp also) inside the network rather than a simple confinement model with selection rule breakdown [13]. The broadening of the bands is due to the bond constraints inside the lattice. Ferrari and Robertson [14] gave a relationship between the position, the width and the intensity ratio of the Raman bands versus the hybridization. They found that the G band is shifted towards low energy, increasing the sp^3 character. At the same time, these authors claimed that the ratio between D and G bands is proportional to the number and clustering of rings, respectively. Other satellite peaks are also observed in the Raman spectra. Two correlated peaks located at 1150 cm^{-1} and 1450 cm^{-1} are attributed to an alternate chain of sp^2 carbon atoms with a single hydrogen bonded to each carbon [15]. Ferrari and Robertson [16] reported sp^3 sites giving in UV excitation a peak located at 1060 cm^{-1}.

Let us examine the case of rich sp^3 amorphous phases called DLC (diamond-like amorphous carbon) and tetrahedral amorphous carbon (ta-C) [17]. Wang and Ho [18] calculated the V DOS of a DLC prepared by molecular dynamics. The four fold atoms (sp^3 hybridized) give a signal ranging between 200 and 1400 cm^{-1} while three fold atoms contribute to the V DOS in the whole range 200 to 1900 cm^{-1}. Their structure contains 80% four fold atoms which explains a large density near the region 1000–1200 cm^{-1}. The band located near 1100 cm^{-1} has been yet reported by Gilkes et al. [19] in ta-C which contains at least 80% of sp^3 sites. This band is emphasized by Raman resonance since the authors operated in UV region. Marks et al. [20] found that ta-C prepared by ab initio molecular dynamics presents 65% of sp^3 sites and a ring statistic where five-fold rings and six-fold rings are of the same order of magnitude, the density of the film being about 3 g/cm^3. These authors mentioned the correlation between the presence of three- and four-membered rings and the sp^3 hybridization. The structure presents some striking similarities with the cycloalkanes that questions the role of the C–H bonding in such networks.

3.2. Silicon

3.2.1. *Fullerene and surface reconstruction*

Silicon presents two main differences from carbon. In silicon, there is a possibility for a repulsive overlapping between the inner $2p$ and the valence $3p$ orbital. On the other hand, a silicon atom can promote in $3d$ shell which favors a coordination greater than four. Finally, silicon prefers a hybridization close to sp^3 above a few tens of atoms. For the smallest sizes, silicon adopts a compact structure as observed in the high pressure regime. Even though Si_{60} has not yet been reported, there are magic number for silicon clusters, the most fascinating being Si_{33} (Fig. 1). The structure is derived from a piece of clathrate Si_{28} with five atoms inside the fullerene Si_{28} [21]. In Si_{28}, the HOMO level is threefold degenerated with four electrons while LUMO is a single state and LUMO + 1 a singlet state located at higher energy. If we bring four electrons, HOMO and LUMO will be completely filled while LUMO + 1 remains empty. The appearance of a new gap (LUMO + 1 − LUMO) gains a new stability. These electrons can be brought by a tetravalent atom inside the cage, four hydrogen atoms outside the cage or four electrons belonging to the Si_5 cluster inside the cage. Two Si_{33} isomers were proposed by Kaxiras et al. [22] and Röthlisberger et al. [23]. In fact, the position of the Si_5 does not play an important role. This is emphasized if we calculate within the local density approximation to the density functional theory (DFT) [24,25] two isomers with two different configurations (Fig. 1). One is deduced from the surface reconstruction of a T_d^1 lattice (Si_{33}^a) the other is deduced from the clathrate structure (Si_{33}^b). The crossing from one to the other is obtained by rotating the

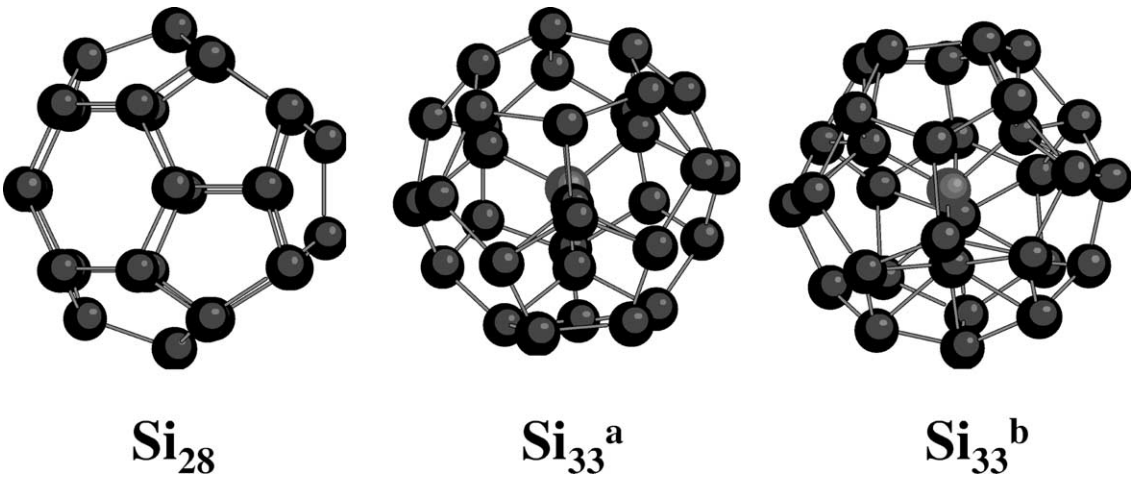

Figure 1. Left: T_d Si_{28} cage belonging to the fullerene family with twelve pentagons and four hexagons. This is the elemental brick of the clathrate structure. Middle and right: two isomers of Si_{33} derived from the addition of Si_5 and Si_{28}.

Si_5 tetrahedron inside the Si_{28} cage. The difference in energy per atom is less than 4 meV lower than the DFT accuracy. [1] We note that in this case, there is no significant rotation barrier, Si_5 still acts as a pseudo 'tetravalent atom'. However, the mean coordinance $\overline{N}$ and the bond lengths differ significantly from the fourfold configuration ($\overline{N} = 3.6$ and 4.2 in Si_{33}^a and Si_{33}^b, respectively). For comparison, a T_dSi_{33} cluster having the diamond structure presents a mean coordination $\widetilde{N} = 3.0$. Consequently, Si cage-like fullerenes will be more dense than the adamantane structure. This of importance for the discussion in Section 7. Above a few hundred of atoms, a silicon cluster adopts the diamond structure. The transition between the diamond structure and the so called 'amorphous state', which also contains the structures discussed above, is known as the thermodynamic instability. The critical size is about 2 nm. Above this size, a silicon cluster crystallizes in the diamond phase and cluster-based materials are well described in terms of the confinement model as mentioned in nanoporous or nanocrystalline silicon [26].

3.2.2. *V DOS in amorphous silicon*

For silicon, the most common model is the Continuous Random Network (CRN) model where bond and dihedral angle distortions affect the tetrahedral diamond structure. In addition, strong constraints on the network are partially released by introducing some defects, such as odd-membered rings, dangling bonds or over coordinated atoms (coordinance > 4). At ground level, the V DOS of a-Si is close to the phonon DOS in diamond structure. Some discrepancies appear at high energies where the a-Si V DOS is shifted towards low energy. When the network is short range well ordered, the selection rules are not entirely broken. We can applied the confinement model, giving rise to Raman bands intermediate between a-Si and silicon crystal. This is observed in nano-porous silicon where the elementary brick (ranging from 2–10 nm) crystallizes in the diamond phase.

3.2.3. *eDOS in amorphous silicon*

In covalent structures, V DOS and eDOS are correlated. eDOS is deduced from the valence band observed by XPS performed at the Fermi level threshold after inelastic scattering and cross section corrections. eDOS in diamond silicon is basically formed by three bands corresponding to s-like (10 eV), sp-like (7.5 eV), and p-like (3.5 eV) characters [27]. Amorphous silicon presents a merging of the sp- and p-like bands. This merging is attributed to five-fold defects in the network [28]. The nanoporous structure

and amorphous valence band are quite similar [29]. The discrepancies between V DOS observed by Raman spectroscopy and eDOS in a-Si and nano porous silicon are interesting. eDOS is sensitive to the defects, while V DOS in Raman is mainly sensitive to the short range order.

4. Silicon–carbon

Silicon carbide is a wide semi conductor sp^3 hybridized as common silicon or diamond with numerous polytypes [30]. Amorphous SiC (a-SiC) has been extensively studied too. They are more or less described in terms of a tetrahedral environment. Si_xC_{1-x} compounds with $x \neq 0.5$ are more complex and still debated since topological and compositional disorders introduce both the homonuclear and heteronuclear bonds. The tendency to chemical ordering into an sp^3 network prevails in Si-rich films, and conversely, the disorder increases in C-rich films [31]. This is easily understood if we remember the electronic structure of the both silicon and carbon atoms. Silicon prefers tetrahedral bonding while carbon prefers three-fold bonding. There is a competition between both types of bonding. In a large cluster, tetrahedral bonding prevails since carbon takes easily a four-fold configuration without a noticeable cost of energy. Decreasing the cluster size, the problem is less obvious. Carbon takes a fullerene-like structure with an empty core while silicon prefers a dense packing as observed in Si_{33}. Even though the structure of Si_nC_m clusters remains misunderstood, a few have been demonstrated in particular the heterofullerenes. SiC heterofullerenes Si_qC_{2n-q} with $2n = 32$–100 and $q < 12$ are obtained by a substitutional doping of carbon with silicon [32]. For example, Si_2C_{58} heterofullerene is derived from the C_{60} parent where two silicon take the place of two carbon atoms (Fig. 2). Such a structure is stable when the silicon/carbon ratio is low enough. The phase transition between a tetrahedral Si–C bonding towards a fullerene like structure is also reported [33]. Starting from nearly stoichiometric Si_xC_{1-x} clusters $x \approx 0.5$, one expects a tetrahedral bonding between Si and C atoms. If we irradiate these clusters with a laser, they fragment and evaporate small Si-rich clusters such as Si_2C or Si_3C. After several evaporation rounds, clusters become strongly carbon rich and then a phase transition occurs

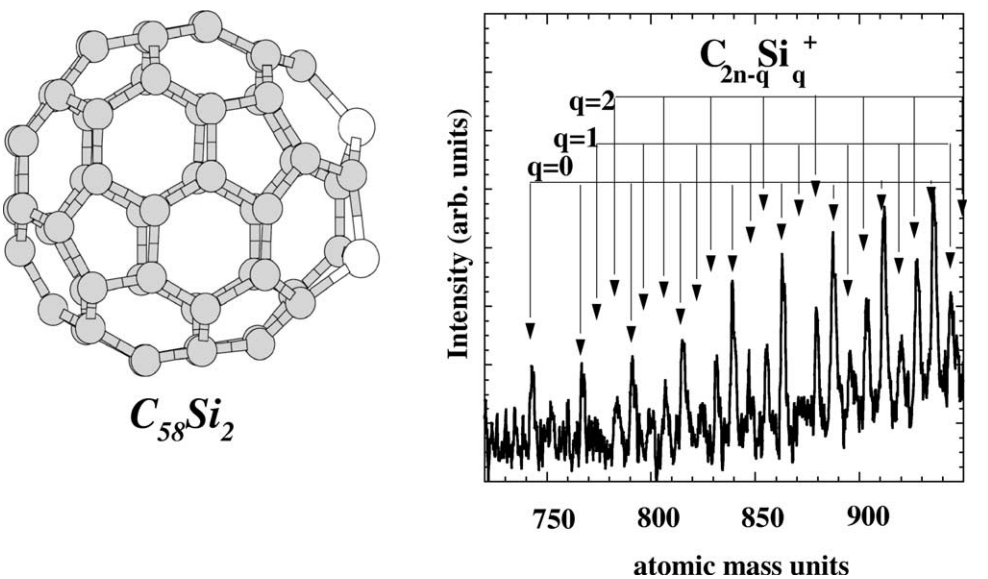

Figure 2. Left: schematic ball and stick picture for the heterofullerene $C_{58}Si_2$. The dark and light atoms are the carbon and silicon, respectively. Right: part of the mass abundance spectrum showing the heterofullerenes. The q number gives the number of silicon atoms inside the heterofullerenes. Upper values $q > 2$ are not yet observed in this spectrum. The upper limit is $q = 12$.

leading to the heterofullerenes. The process stops when silicon atoms have totally disappeared. Afterwards, the fullerenes evaporate a C_2 molecule following the classical process $C_{2n} \rightarrow C_{2n-2} + C_2$.

5. Experimental outlook

Silicon, carbon or silicon–carbon mixed clusters are formed in a standard laser vaporization source. Further information is given in an earlier paper [33]. The mean stoichiometry x of the clusters Si_xC_{1-x} is governed by the initial composition of the target. We use composite rods processed by binding silicon and graphite powders in various proportions. We also use a double-target laser vaporization source [34] for specific applications (C_{60}–Si, see below). Prior to deposition, the cluster size distribution is measured in a high resolution time-of-flight spectrometer equipped with a reflectron device. Neutral clusters are photoionized by a pulsed ArF excimer laser with a 6.4 eV photon energy. In addition to mass spectrometric measurements, photofragmentation experiments on selected clusters sizes have been carried out. Neutral clusters are deposited in an ultra high vacuum chamber and then transferred in situ in a dual XPS/Auger CAMECA Nanoscan 100 type microprobe. XPS measurements are performed using Al K_α x-rays (1486.6 eV) with a photoelectron energy resolution fixed at 1 eV. For Auger and electron energy loss (EELS) spectroscopies, the primary electron energy is fixed at 2 keV. During cluster deposition, the vacuum was down to 2×10^{-7} Pa mainly due to the residual buffer helium gas. The total pressure of other reactive components (O_2, CO, H_2O, CO_2, ...) was less than 10^{-8} Pa. The film thickness is about 50 nm and corresponds roughly to the stacking of 50–100 cluster monolayers. The substrate is a silicon wafer (111) coated with a thick silver film (200 nm) previously evaporated in-situ. Our samples are compared with other reference samples, namely a (111) silicon single crystal (labelled Si-2), a silicon clathrate (labelled Si-34), a hydrogenated amorphous silicon (labelled a-Si:H), a hexagonal silicon carbide (labelled 2H–SiC), a C_{60}-cluster film [2] and a freshly cleaved HOPG graphite. Raman spectrometry measurements are performed at room temperature using a DILOR XY confocal micro-Raman spectrometer. The clusters are deposited onto a 2 mm thick cleaved lithium fluoride (LiF) substrate, then coated with a 100 nm thick silver film [35]. The thickness of the deposited film is about 50 nm. Such a sample geometry allows a Raman measurement through the highly transparent LiF substrate, the silver film deposited on top acting as a protection barrier. Raman spectra are excited in the direction normal to the sample using 514.5 nm or 288 nm lines. The scattered light is also collected in the direction normal to the sample. The interface between the silver coating and the heterofullerene film is at the origin of a 'Surface-Enhanced Raman Scattering' (SERS) effect very convenient for analyzing our samples with the lowest possible laser fluence [27]. For silicon compounds, Si K-edge absorption spectra were recorded collecting the total drain current or the fluorescence as a function of the photon energy. The measurements were performed on beam line SA32 (located on the 800 MeV positron storage ring SuperACO in Orsay). The x-ray beam was monochromatized by an InSb double crystal monochromator (0.7 eV resolution).

6. Carbon cluster based materials

Carbon cluster-based films observed in AFM mode appear nanostructured [36,37]. The density of the film measured by Rutherford Backscattering and Talystep together ranges around 0.8–1 g/cm^3 far away from the density of carbon-based materials (around 3 g/cm^3). Our film could be compared to a nanosponge with a large part of under coordinated atoms. Such a feature has been already observed by Milani et al. [37] using a pulsed micro-plasma cluster source. Figs. 3c and 3d display the Raman spectra and the corresponding size distributions for $N_{\text{mean}} = 32$ atoms. We use photons at 266 nm in order to excite σ states of sp^3 sites. The Raman signal is arbitrary decomposed in four components labelled T_1, T_2, G and D, respectively. Earlier measurements performed in visible region (514 nm) gave the same bands with different relative intensities [38]. By comparison with the literature data, G and D bands yield the collective features of both the sp^2 and the sp^3 atoms. The T_1 band is observed in [18,19] t-aC or DLC (see Section 3.1). Nevertheless, the similiarity between t-aC and LECBD-films does not hold further. The density of our

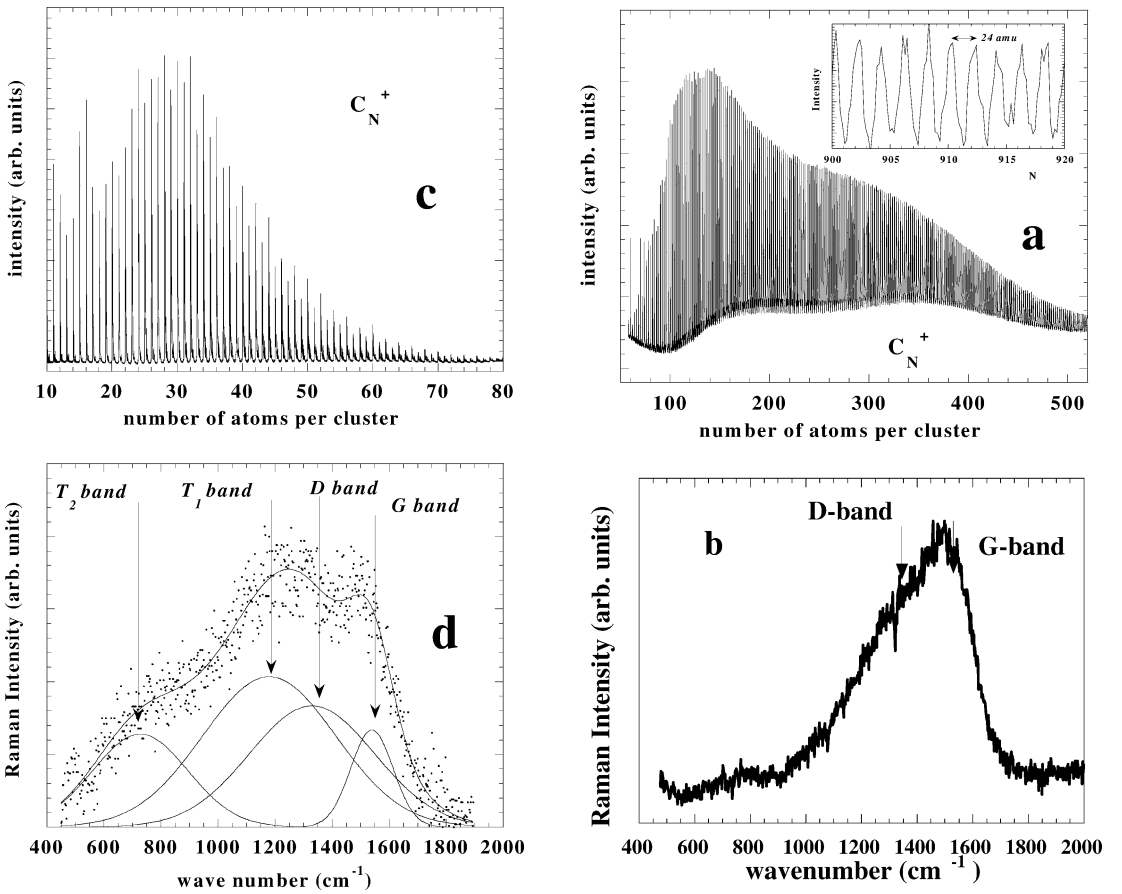

Figure 3. (a) Mass abundance spectrum of large carbon clusters with an insert showing the 24 amu periodicity up to $N = 1000$ atoms. (b) First Raman spectrum (266 nm excitation line) of the film obtained by deposition of the free clusters showing in (a). (c) Mass abundance spectrum of small carbon clusters. (d) First Raman spectrum (266 nm excitation line) of the film obtained by deposition of the free clusters showing in (a).

film is about 0.8–1 g/cm^3 and the film is *hydrogen free* discarding the cycloalkane contribution [20]. As mentioned above, following Ferrari et al., the sp^3 content is rather correlated to the G band position and the peak located at 1060 cm^{-1}. Unfortunately, our spectra exhibit broad bands that contain all the possible configurations. However, the position of the G band is significantly lower (near 1500 cm^{-1}) than those observed in a-C compounds (1520–1580 cm^{-1}) that corroborates a large sp^3 content. We observe striking similarities with the Raman signal and the V DOS calculated by Wang and Ho [18]. Canning et al. [40] studied by molecular dynamics thin films produced by the deposition of C_{28} fullerenes not so far from our mean cluster size. These authors found a remarkable stability of the film despite a large void fraction, the density being no more than 1 g/cm^3. In addition, Galli et al. [41] calculated allowed Raman and infrared frequencies of several C_{20} isomers (rings, planar and fullerenes). A signal ranging 1000–1200 cm^{-1} characterizes the C_{20} fullerene. Such features suggest that the neutral clusters present various shapes and isomers and in particular fullerene-like structure. We underline that the competition between the isomeric forms depends on the nucleation regime. If we modify the nucleation parameters (helium pressure, laser power,...) we gets cluster-assembled films without significant T_1 and T_2 bands. In this case, the gap is lower and the conductivity much more. Nevertheless, no available information between the relative cross

sections for $T_{1,2}$, G and D bands permits a quantitative estimation of sp^3 bonding in our film. A crude model give rises to a large sp^3 sites as defined in Eq. (1). However, the sp^3 hybridized atoms are confirmed by EELS measurements suggesting a very weak contribution of $\pi - \pi*$ bonding. Moreover, conductance and optical data show the existence of a band gap and a low conductivity in such films. Finally, in the framework of the 'memory effect' assumption, we expect that a part of carbon clusters present a fullerene-like structure as shown in Fig. 1 (left panel, i.e. C_{28}). Following Ferrari et al., T_1 and T_2 bands contain all the feature that characterize sp^3 (1060 cm^{-1}) and sp^2 (1150 cm^{-1}). Nevertheless, the large broadening of the bands rules out a direct comparison with common amorphous phases. We refer to the density of states in t-aC or fullerene deposition and suggests that T_1 and T_2 bands are assigned to a sp^3-like component. Such bands cancel out when increasing the cluster size (see Eq. (1)). Figs. 3a and 3b display the size distribution and the corresponding Raman spectra for bigger clusters namely $N_{\text{mean}} = 100$–400 atoms. We observe a remarkable even parity for carbon clusters for the biggest clusters (see insert Fig. 3a). This parity (24 amu) is often evoked as the fullerene-like signature. The first amazing result is the even parity up to 1000 atoms and more. This questions the true structure of the clusters. We discard the fullerene-like structure since such large fullerenes give rise to wide open structures giving very small films densities. The film density is about 1 g/cm^3 as observed for smallest sizes. The structure is still more complex than that observed, for example, in onion structures. However, according to the expected structure: fullerenes or onion fullerenes (i.e. fullerenes with one single wall or more), the number of pentagons decreases with the size and the hybridization must tend to $n = 2$ (see Eq. (1)). This is clearly observed since G and D bands which characterize sp^2/sp^3 mixing and disorder are present, while the T_1 Raman band at 1000–1200 cm^{-1} cancels out. The broadening of both the G and the D bands should be explained by the spread in the deposited cluster sizes. Each fullerene gives rise to particular modes (for example in C_{60} $A_g = 1469$ cm^{-1}) beneath those observed in graphite ($A_g = 1581$ cm^{-1}). The softening is due to the constraint energy and is related to the so called mean hybridization defined in Eq. (1). Even though the features present some striking similarities with a-C, we do not invoke the presence of fused rings linked by tetrahedral carbon atoms in the LECBD films.

7. Silicon cluster based materials

Fig. 4b displays HRTEM pattern of a silicon cluster-based film (Si-film). The corresponding size distribution is shown in Fig. 4a. Most of the clusters are smaller than the critical size (around 2 nm) where the diamond structure becomes unstable. After surface reconstruction, we expect structures having some similarities with the Si_{33} model developed above. The film appears nanogranular, each supported grain size corresponding almost to one in free phase suggesting a weak coalescence regime. The density of the film is 50–70% that observed in the crystalline phase or in a-Si compounds. The inner structure observed by direct imaging or by nano-diffraction appears amorphous-like. The inner structure is then studied by EXAFS performed at the Si K edge. Fig. 4c displays the pseudo radial distribution obtained for the Si-film compared to crystalline phases (diamond and clathrate) and amorphous structure (a-Si:H). One observes that in all cases, the silicon atoms in Si-film and a-Si:H are under coordinated with respect to the Si-2 phase. The under coordination in a-Si:H has already been observed [42,43] and has been assigned [42] to Si–H bonds not detected by EXAFS. In addition, a large under coordination ($N \ll 4$) has been reported for porous silicon structures [44] having a density comparable to our films. In the case of the silicon-cluster assembled film, the origin of this under coordination is different, since all our experiments are made in ultra high vacuum without noticeable hydrogen. Even though we can not rule out the presence of a few Si–H bonds, the most important effect comes from dangling bonds. However, the most striking result is the slight difference between the coordination of the silicon in Si-film and a-Si:H and the large value compared to porous structures. The density of our films is half that observed in a-Si:H compounds. Since EXAFS gives the mean coordinance averaged for all silicon atoms, we can believe that silicon clusters are partially connected to each other and probably over coordinated with respect to the ideal value $N = 4$ in

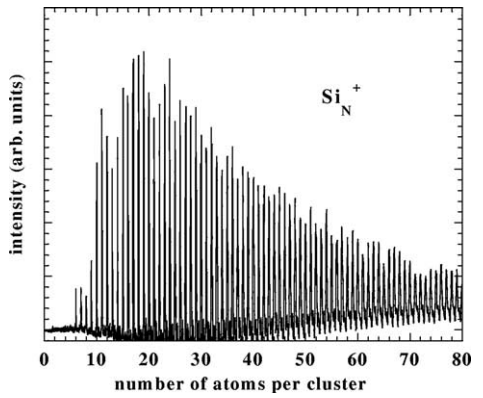

(a)

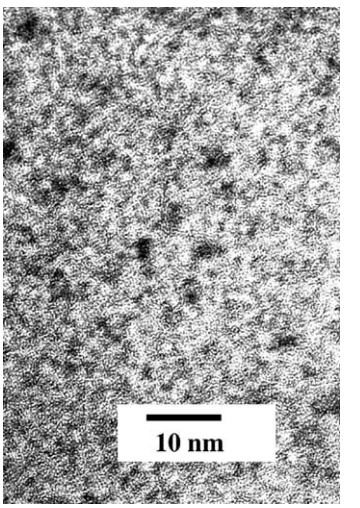

(b)

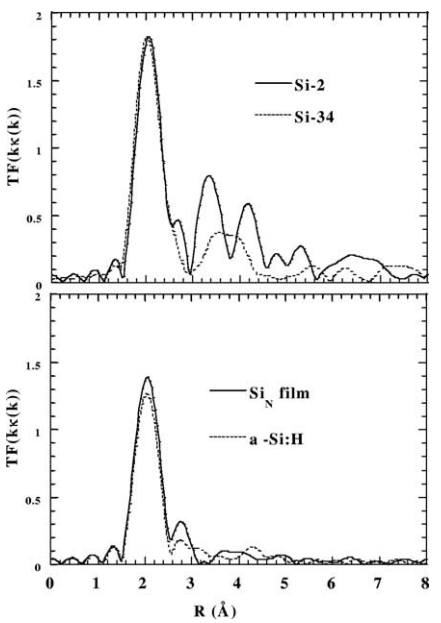

(c)

Figure 4. (a) Mass abundance spectrum of small silicon clusters. (b) HRTEM micrograph obtained with a 20 nm thin film deposited on an a-C coated grid. (c) Upper: pseudo radial distribution function of Si-2 and clathrate (labelled Si-34) crystals. The amplitude of the main peak corresponds to the first shell with a coordination $N = 4$. Lower: pseudo radial distribution function of the cluster-film and a-Si:H film. We clearly observed that the mean coordination number in the cluster-film is greater than the one in a-Si:H and is close to those observed in crystalline forms.

the diamond phase (see Section 6). This agrees with the over coordination expected in silicon clusters such as Si_{33} cluster for example. Fig. 5a displays the eDOS for the Si-film compared to Si-2 and clathrate. This latter is interesting since clathrate is formed by a triplicate periodic arrangement of Si cages with 87% of five fold rings (Si-2 being formed by six-fold rings). The position of the $3s$ and $3p$ bands is affected by the oddness and give us a reference for the five-fold defects in the Si-cluster film (we have to remember that five fold rings are present in small clusters such as Si_{33}). The eDOS in the Si-film is similar to the one observed in a-Si with p-like sp-like bands merging. This is unambiguously attributed to the five-fold/six -fold rings mixture in our Si-films [27]. Fig. 5b displays the V DOS deduced from Raman spectroscopy. We have

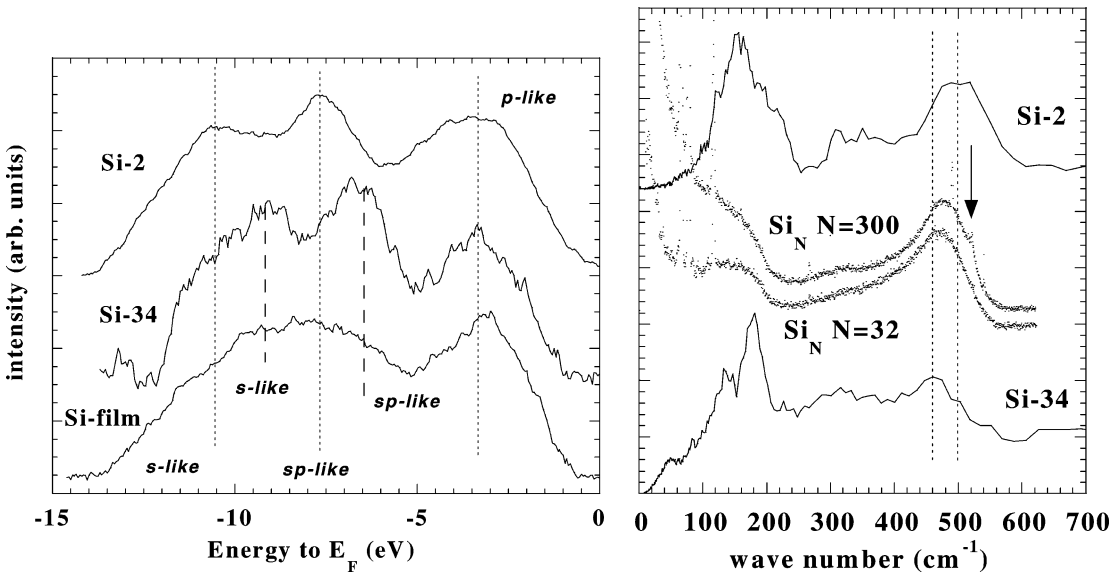

Figure 5. (a) Valence band for Si-2, clathrate and cluster-film. Each subband is assigned. These spectra obtained by XPS spectroscopy near the Fermi level are corrected for the inelastic scattering tail. (b) Phonon density of states deduced from neutron scattering measurements (Si-2 and Si-34 clathrate). First order Raman spectra (excitation line 514.5 nm) measured at room temperature in the crossed polarization mode for two cluster-films (mean cluster sizes, $N = 32$ and $N = 300$, respectively). The small bump marked by an arrow on the Si_{300}-film spectrum indicates the presence of a crystalline component in this sample.

also displayed the V DOS for Si-2 and clathrate measured by inelastic neutron scattering [45]. At ground level, the Si-cluster film presents some similarities to the a-Si, indicating no short range order (in agreement with the EXAFS spectra). The position of the maximum (near 470 cm^{-1}) is intermediate between Si-2 and clathrate. This indicates a mixing between five-fold and six-fold rings. Fig. 5 also displays the V DOS of larger clusters ($N_{mean} = 300$ atoms) where the five fold rings ratio is less. We observe a slight shift towards high energy (478 cm^{-1}) (i.e. more six-fold rings) with a weak signal at 521 cm^{-1}. This corresponds to larger silicon clusters above the limit of stability which are crystallized. In summary, Si-films are very similar to a-Si phases despite a very low density. The low density and the film morphology discards the continuous random network (CRN) as a realistic model for Si LECBD films. We can expect Si clusters having a complex structure based from five-fold/six-fold rings mixture. It is unlikely that any such silicon network will succeed in perfectly closed shell like in Si_{33} cluster, this latter being just a crude model.

8. Silicon–carbon mixed cluster based materials

As mentioned above, the properties strongly depend on the silicon/carbon ratio. We present three different cases 50/50, 12/88 and 2/98 ratios, respectively. As mentioned previously, $x = 0.12$ corresponds to the deposition of heterofullerenes. Prior to the discussion, we have to mention that the mean stoichiometry of the supported clusters just coincides with the initial target used for the vaporization. This is of importance for the following discussion.

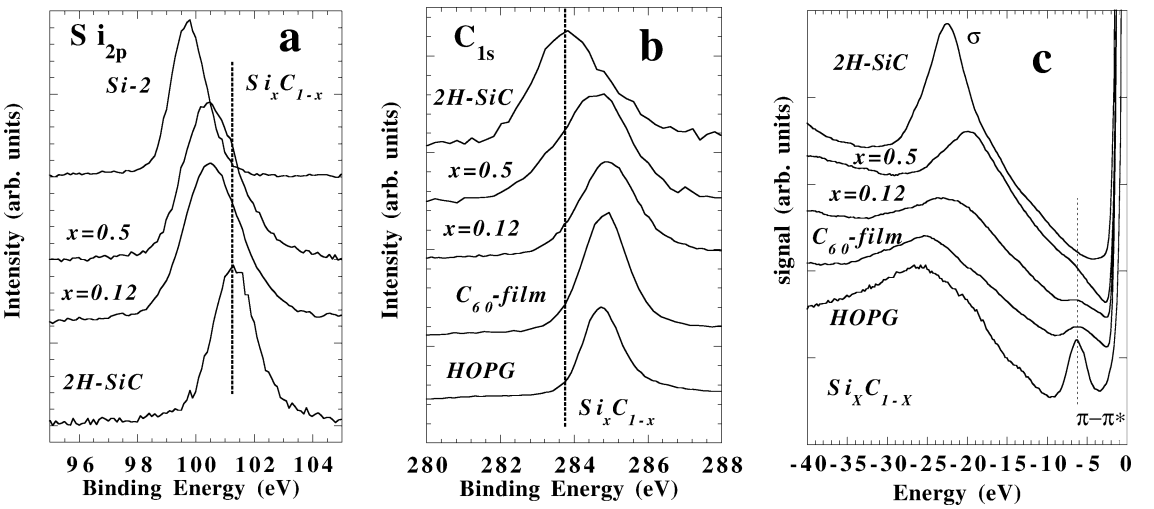

Figure 6. (a) Si_{2p} core level lines for several samples, Si-2, 2H–SiC, Si_xC_{1-x} $x = 0.5$ and Si_xC_{1-x} $x = 0.12$, respectively. (b) C_{1s} core level lines for several samples, HOPG, 2H–SiC, C_{60}-film, Si_xC_{1-x} $x = 0.5$ and Si_xC_{1-x} $x = 0.12$, respectively. (c) Plasmon losses observed in EELS spectroscopy for various samples, HOPG, 2H–SiC, C_{60}-film, Si_xC_{1-x} $x = 0.5$ and Si_xC_{1-x} $x = 0.12$, respectively.

8.1. Electronic structure

Nucleation in the source obeys a statistical combination between Si–Si, Si–C and C–C atoms [46]. Consequently, deposited clusters present a spread in sizes and compositions. TEM and electron diffraction reveal an amorphous-like structure without well-ordered nano particles [47]. Figs. 6a and 6b display the Si_{2p} and C_{1s}, respectively, core level lines in various samples. We clearly show that Si_{2p} core level lines in Si_xC_{1-x} for $x = 0.12$ and $x = 0.5$ are at the same position and are located between the Si_{2p} lines observed in wurtzite 2H–SiC and Si-2, respectively. The C_{1s} line in Si_xC_{1-x} ($x = 0.12$ just coincides) with those observed in HOPG graphite or C_{60}-film obtained by the deposition of pure C_{60} clusters. C_{1s} core level line in Si_xC_{1-x} ($x = 0.5$) is broadened and shifted towards the C_{1s} line in wurtzite 2H–SiC (the atoms are tetrahedrally bonded). A careful analysis reveals that C_{1s} core level lines can be decomposed in two components, mainly C–C and Si–C bands. For $x = 0.5$, the signal is formed by the juxtaposition of both the C–C bonding like observed in HOPG (sp^2-like) and the Si–C bonding like observed in 2H–SiC (sp^3-like). Conversely, for $x = 0.12$, the signal arises from C–C bonding as observed in HOPG. This indicates that carbon bonding differs in both samples ($x = 0.12$, $x = 0.5$). This is emphasized in Fig. 6c, displaying the plasmon bands. The main plasmon band is located at low energy for $x = 0.5$. This is due to the lower density of the film for $x = 0.5$ since the Si–C bonding distance is larger than the C–C bond (the occurrence of Si–C bonding increases with x). The most interesting result is the softening of the π–$\pi*$ bonding giving the sp^2 character. The Si_xC_{1-x} ($x = 0.12$) corresponding to the deposition of the heterofullerenes has a lower sp^2 character than graphite and C_{60}-film. Si_xC_{1-x} ($x = 0.5$) shows a small shoulder in the π–$\pi*$ region indicating a weak sp^2-like character in agreement with the XPS data.

8.2. Vibrational structure

Fig. 7 displays the Raman spectrum at low laser fluence ($P < 1$ mW) corresponding to $x = 0.5$. We observe three regions corresponding to C–C, Si–C and Si–Si vibrational modes. The carbon region is formed by both the *G* and the *D* bands as observed for carbon clusters (Figs. 2b and 2d). The silicon region corresponds to the one observed for silicon clusters (see Fig. 5b). Finally, the Si–C region corresponds to the silicon (carbon, respectively) located at the interface with the carbon (silicon, respectively) in the

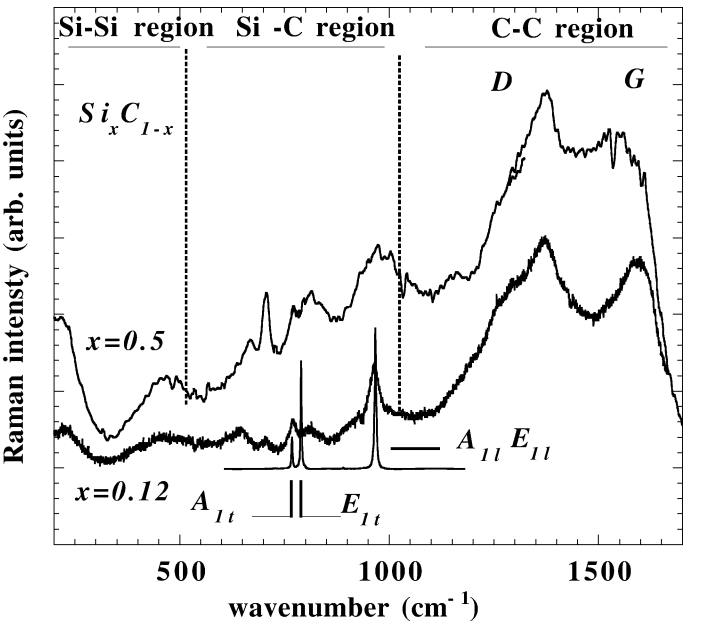

Figure 7. First order Raman spectra (514.5 nm excitation line) for Si_xC_{1-x} $x = 0.5$ and Si_xC_{1-x} $x = 0.12$, respectively. Raman allowed modes corresponding to 2H–SiC are also displayed. Such modes corresponding to Si–C bonding just coincides with the bands assigned to 'Si–C region'.

cluster. All these features suggest a nonchemical ordering inside the cluster and corroborates the broad band observed in C_{1s} region (Fig. 6). Such a feature is often reported in a-SiC, where the chemical ordering which prevails in the crystalline phase is partially destroyed. As mentioned previously, the main reason is the difference between carbon and silicon. Carbon prefers three-fold coordination while silicon prefers four-fold coordination. This dilemma is partially solved by a so called 'phase separation'. For $x = 0.12$ no noticeable signal is observed in the Raman spectrum of the cluster film in the 500–1000 cm^{-1} region corresponding to the phonon density of states. However, the Raman signal appears clearly (Fig. 7) by increasing the laser power up to 10 mW (the laser spot diameter on the sample is about 2–4 mm). This signal is attributed to the phototransformation of the sample under laser irradiation [48] leading to a darkening of the irradiated area. The spectrum reported corresponds to a steady state (at 10 mW) where any band does not significantly changes. The bands are very similar to those observed in Si_xC_{1-x} sample ($x = 0.5$). Nevertheless, it seems that the sharpening of the Si–C bands for $x = 0.12$ suggests a well ordered Si–C region after photo-transformation.

8.3. C_{60}–Si based material

We have studied the doping of fullerenes or carbon network by substitutional silicon atoms [49]. Another way is the doping by intercalating silicon atoms between the pure carbon fullerenes. For this purpose, we co-evaporate pure C_{60} and silicon atoms together in the laser vaporization source [34]. The laser fluence is not enough to destroy the C_{60} inner structure. The size distribution shows mixed fullerenes corresponding to the whole formula $(C_{60})_xSi_{1-x}$. After deposition, Raman spectroscopy show unambiguously that C_{60} molecules survive after collision with the substrate. Fig. 8 shows the experimental $\chi(k)$ of the C_{60} + Si (curve (c)) sample deduced from EXAFS, to be compared with Si-2 (curve (a)) and 2H–SiC (curve (b)). The pseudo radial distribution function $g(R)$ of the C_{60} + Si sample (i.e. the Bessel Fourier transforms of $k^3\chi(k)$), is also given in Fig. 8f. The first striking feature observed in the C_{60} + Si sample is that $\chi(k)$ is remarkably well structured as shown by the oscillation of $\chi(k)$ up to 11 $Å^{-1}$, and the features of $g(R)$ up to 5 Å. Secondly, silicon atoms in the C_{60} + Si sample are obviously not in the same local environment as in Si-2 or 2H–SiC. Instead, we can think of a silicon surrounded by C_{60} molecules, since the C_{60} survive after deposition. $g(R)$ displays three shells, the one located at 2.2 Å and 3.5 Å respectively are related to

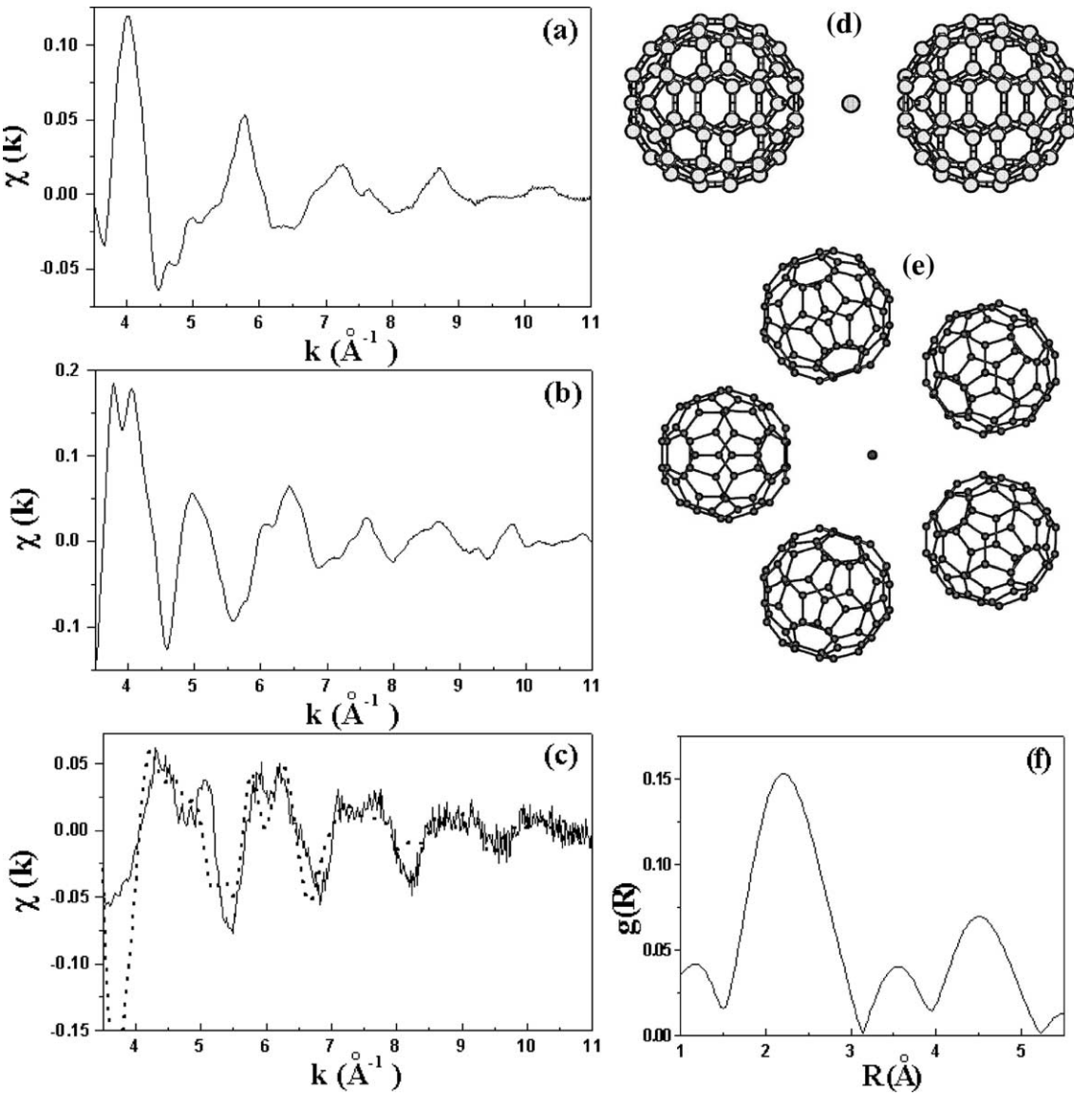

Figure 8. Experimental EXAFS signals $\chi(k)$, of (a) Si-2, (b) 2H–SiC, and (c) the C_{60} + Si film. Pair radial distribution function $g(R)$, of C_{60} + Si film is also displayed (f). For C_{60} + Si film, the experimental data are in continous line, the dashed line giving the fit with the model displayed in the Figs. 8d (Oz axis) and 8e (Oxy plane) (see text). For the calculation, we use self consistent FEFF-8 code [55].

the first and second carbon neighbors. As shown below, $\chi(R)$ can be well fitted assuming the contribution of two C_{60} located on both sides of silicon. The third peak located at 4.5 Å is also unusual and implies carbon atoms at large distances. After simulation using all the configurations derived from the classical intercalated-fullerites structures, the best fit corresponds to a silicon atom between two C_{60} and surrounded by five C_{60} forming a regular pentagon (see Figs. 8d and 8e). This structure forms a decahedron which has been already speculated [50] in $(C_{60})_N$ clusters in free phase. The proposed structure get rises to two nearest C_{60}, facing the silicon atom with a pentagonal face (10 nearest neighbors, $d_{SiC} = 2.52$ Å). To

study the stability and electronic properties, we perform ab initio calculations, within the local density approximation to the density functional theory (DFT) [24,25] on two C_{60} molecules with a Si atom. [3] The role of the five C_{60} is not discussed here. Upon relaxation, the pentagonal structure is found to be stable with a slight deformation of the C_{60} and a small offset of the Si atom from the center position. The distance between Si and the carbon atoms of the pentagonal faces, d_{SiC}, varies from 2.57 Å to 2.62 Å, with a mean distance $d_{SiC} = 2.59$ Å. This value is in good agreement with the results of the EXAFS simulations. The cohesive energy of the relaxed structure, compared to two relaxed C_{60} molecules plus a silicon atom infinitely far from one another, is about 2 eV, much more than the VdW bonding.

9. Discussion/conclusions

LECBD technique is a powerful method for the synthesis of new materials. Contrary to other methods where the films grow on the substrate by addition of atoms or molecules, LECBD films grow by stacking of preformed clusters in free phase without noticeable rearrangement (except for C_{60} + Si). The structure of the free cluster is mainly governed by the surface/volume ratio. For the particular case of covalent clusters, the dangling bonds involve a surface reconstruction. This surface reconstruction leads to several isomers with different hybridizations for carbon or possible dense phases (coordination number greater than four) with five-fold rings in silicon. Mixed SiC clusters present several configurations following the Si/C ratio. For $x = 0.5$, a phase separation is observed. At low x values, the structure is governed by the carbon with a phase transition leading to heterofullerene structure. Finally, we can associate C_{60} molecules with silicon atoms leading to unusual bonding (silicon is surrounded by ten carbon atoms). Such films are not limited to covalent atoms. We can also associate metal and covalent atoms. The most famous example is the 'fullerene' cage Ti_8C_{12}. Work is in progress for the synthesis of new materials.

[1] The present calculations are first performed within the local density approximation to the DFT. A standard pseudopotential is used for Si and the wave functions are expanded on a plane-wave basis with kinetic energy up to 16 Ry.

[2] A C_{60}-cluster film is obtained by deposition of C_{60} packing clusters.

[3] We adopt a pseudopotential approach [51,52] and a numerical-atomic-orbitals (NAO) expansion of the wavefunctions. While a DZP basis has been adopted for Si, a DZ basis was found to be accurate enough for C atoms (see [53] and references therein) using the SIESTA code [54].

Acknowledgements. The authors thank Professor B. Champagnon (LPCML, Université Claude Bernard, Lyon, France) and Doctor V. Paillard (LPS, Université Paul Sabatier, Toulouse, France) who performed the Raman spectroscopy. EXAFS measurements have been made at LURE facility (Orsay, France) with the collaboration of Doctors A.M. Flank and P. Lagarde. The authors wish to thank Doctor X. Blase for very useful discussions and help with the DFT code. We also thank O. Boisron and G. Guiraud for valuable technical assistance.

References

[1] M. Nirmal, L. Brus, Acc. Chem. Res. 32 (1999) 407.
[2] Z. Iqbal, S. Veprek, J. Phys. C 15 (1982) 377.
[3] H.W. Kroto, J.R. Heath, S.C. O'Brien, R.F. Curl, R.E. Smalley, Nature (London) 318 (1985) 162.
[4] C. Cros, M. Pouchard, P. Hagenmuller, J.S. Kasper, Bull. Soc. Chim. France 7 (1968) 2637, 2 (1971) 379.
[5] P. Mélinon, V. Paillard, V. Dupuis, A. Perez, P. Jensen, A. Hoareau, J.P. Perez, J. Tuaillon, M. Broyer, J.L. Vialle, M. Pellarin, B. Baguenard, J. Lerme, Int. J. Mod. Phys. B 139 (1995) 339.
[6] G. Fuchs, P. Mélinon, F. Santos Aires, M. Treilleux, B. Cabaud, A. Hoareau, Phys. Rev. B 44 (1991) 3926.
[7] L. Bardotti, P. Jensen, A. Hoareau, M. Treilleux, B. Cabaud, Phys. Rev. Lett. 74 (1995) 4694.
[8] J.M. Hunter, J.L. Fye, J. Roskamp, M.F. Jarrold, J. Phys. Chem. 98 (1994) 1810.
[9] G. von Helden, M.T. Tsu, N. Gotts, M.T. Bowers, J. Phys. Chem. 97 (1993) 8182.
[10] Advanced Series in Fullerenes, Vol. 1–5, Word Scientific, Singapore, 1992-1997.
[11] R.C. Haddon, J. Am. Chem. Soc. 108 (1986) 2837.

[12] M. Yoshikawa, N. Nagai, M. Matsuki, H. Fukuda, G. Katagiri, H. Ishida, A. Ishitani, I. Nagai, Phys. Rev. B 46 (1992) 7169, and references therein.
[13] M.L. Theye, V. Paret, A. Sadki, Diamond and Related Materials 10 (2001) 182.
[14] A.C. Ferrari, J. Robertson, Phys. Rev. B 61 (2000) 14005.
[15] A.C. Ferrari, J. Robertson, Phys. Rev. B 63 (2001) 121405R.
[16] A.C. Ferrari, J. Robertson, Phys. Rev. B 64 (2001) 754141.
[17] D.R. McKenzie, D. Muller, B.A. Pailthorpe, Phys. Rev. Lett. 67 (1991) 773.
[18] C.Z. Wang, K.M. Ho, Phys. Rev. Lett. 71 (1993) 1184.
[19] K.W.R. Gilkes, H.S. Sands, D.N. Butchelder, J. Robertson, W.I. Milne, Appl. Phys. Lett. 70 (1997) 1980.
[20] N.A. Marks, D.R. McKenzie, B.A. Pailthorpe, M. Bernasconi, M. Parinello, Phys. Rev. B 54 (1996) 9703.
[21] P. Mélinon, P. Kéghélian, B. Prével, A. Perez, G. Guiraud, J. LeBrusq, J. Lermé, M. Pellarin, M. Broyer, J. Chem. Phys. 107 (1997) 10278.
[22] E. Kaxiras, Phys. Rev. Lett. 64 (1990) 551.
[23] U.R. Hothlisberger, W. Andreoni, M. Parinello, Phys. Rev. Lett. 72 (1994) 665.
[24] P. Hohenberg, W. Kohn, Phys. Rev. 136 (1964) 864.
[25] W. Kohn, L.J. Sham, Phys. Rev. 140 (1965) 1133.
[26] M. Ehbrecht, B. Kohn, F. Huisken, M.A. Laguna, V. Paillard, Phys. Rev. B 56 (1997) 6958.
[27] P. Mélinon, P. Kéghelian, X. Blase, J. LeBrusc, A. Perez, E. Reny, C. Cros, M. Pouchard, Phys. Rev. B 58 (1998) 12590, and references therein.
[28] J.D. Yohannopoulos, M.L. Cohen, Phys. Rev. B 7 (1973) 2644.
[29] R.P. Vasquez, R.W. Fathauer, T. George, A. Ksendzov, T.L. Lin, Appl. Phys. Lett. 60 (1992) 1004.
[30] D. Emin, T.L. Aselage, C. Woods (Eds.), Novel Refractory Semiconductors, MRS Symposia Proceedings, No 97, Materials Research Society, Pittsburgh, 1987.
[31] A. Chehaidar, R. Carles, A. Zwick, C. Meunier, B. Cros, J. Durand, J. Non-Cryst. Solids 169 (1994) 37.
[32] C. Ray, M. Pellarin, J. Lermé, J.L. Vialle, M. Broyer, X. Blase, P. Mélinon, P. Kéghélian, A. Perez, Phys. Rev. Lett. 80 (1998) 5365.
[33] M. Pellarin, C. Ray, J. Lermé, M. Broyer, X. Blase, P. Khéghelian, P. Mélinon, A. Perez, J. Chem. Phys. 110 (1999) 6927.
[34] M. Pellarin, C. Ray, J. Lermé, J.L. Vialle, M. Broyer, P. Mélinon, J. Chem. Phys. 112 (2000) 8436.
[35] P. Mélinon, P. Kéghélian, B. Prével, V. Dupuis, A. Perez, B. Champagnon, Y. Guyot, M. Pellarin, J. Lermé, M. Broyer, J.L. Rousset, P. Delichère, J. Chem. Phys. 108 (1998) 4607.
[36] V. Paillard, P. Mélinon, J.P. Perez, V. Dupuis, A. Perez, J.L. Loubet, H. Pascal, A. Tonck, M. Fallavier, Nanostructured Materials 4 (1994) 759.
[37] P. Milani, P. Piseri, E. Barbonrini, A. Podesta, C. Lenardi, J. Vac. Sci. Technol. A 19 (2001) 2024.
[38] V. Paillard, P. Mélinon, V. Dupuis, J.P. Perez, A. Perez, Phys. Rev. Lett. 71 (1993) 4170.
[39] A.C. Ferrari, B. Kleinsorge, G. Adamopoulos, J. Robertson, W.I. Milne, V. Stolojan, L.M. Brown, A. LiBassi, B.K. Tanner, J. Non-Cryst. Solids 266 (2000) 740.
[40] A. Canning, G. Galli, J. Kim, Phys. Rev. Lett. 78 (1997) 4442.
[41] G. Galli, F. Gygi, J.C. Golaz, Phys. Rev. B 57 (1998) 1860.
[42] A. Filipponi, F. Evangelisti, M. Benfatto, S. Mobilio, C.R. Natoli, Phys. Rev. B 40 (1989) 9636.
[43] M. Wakagi, K. Ogata, A. Nakano, Phys. Rev. B 50 (1994) 10666.
[44] S. Schuppler, S.L. Friedman, M.A. Marcus, D.L. Adler, Y.H. Xie, F.M. Ross, T.D. Harris, W.L. Brown, Y.J. Chabal, L.E. Brus, P.H. Citrin, Phys. Rev. Lett. 72 (1994) 2648.
[45] P. Mélinon, P. Kéghelian, A. Perez, B. Champagnon, Y. Guyot, L. Saviot, E. Reny, C. Cros, M. Pouchard, A.J. Dianoux, Phys. Rev. B 59 (1999) 10099.
[46] P. Mélinon, P. Kéghélian, A. Perez, C. Ray, J. Lermé, M. Pellarin, M. Broyer, M. Boudeulle, B. Champagnon, J.L. Rousset, Phys. Rev. B 58 (1998) 16481.
[47] P. Mélinon, P. Kéghélian, A. Perez, J.L. Rousset, A.M. Cadrot, A. Malhomme, A.J. Renouprez, F.J. Cadete Santos Aires.
[48] P. Zhou, Z.H. Dong, A.M. Rao, P.C. Eklund, Chem. Phys. Lett. 211 (1993) 337.
[49] F. Tournus, B. Masenelli, P. Mélinon, X. Blase, A. Perez, M. Pellarin, M. Broyer, A.M. Flanck, P. Lagarde, submitted.
[50] T.P. Martin, U. Näher, H. Schaber, U. Zimmermann, Phys. Rev. Lett. 70 (1993) 3079.
[51] N. Troullier, J.L. Martins, Phys. Rev. B 43 (1991) 1993.
[52] K. Kleinman, D.M. Bylander, Phys. Rev. B 48 (1982) 1425.
[53] D. Sánchez-Portal, E. Artacho, J.M. Soler, J. Phys.: Condens. Matter 8 (1996) 3859.
[54] D. Sánchez-Portal, P. Ordejón, E. Artacho, J.M. Soler, Int. J. Quantum Chem. 65 (1997) 453.
[55] A.L. Ankudinov, B. Ravel, J.J. Rehr, S.D. Conradson, Phys. Rev. B 58 (1998) 7565.